Coupling of mixed layer processes and thermocline variations in the Arabian Sea

K. V. Ramesh[1] and R. Krishnan

Climate and Global Modeling Division, Indian Institute of Tropical Meteorology, Pune, India

Received 1 June 2004; revised 7 November 2004; accepted 4 February 2005; published 7 May 2005.

[1] This study presents an analysis of observed data sets from multiple sources, including observations from a network of Argo floats during (2002–2003), with the aim of investigating the role of the southwest monsoon circulation in affecting the interactions between the oceanic mixed layer and the underlying thermocline in the northern Indian Ocean. Examination of the seasonal cycle of the upper-ocean thermal structure shows that the surface cooling of the Arabian Sea, during the southwest monsoon season, is accompanied by significant warming of the thermocline. It is seen that the thermocline is warmer by about 1.2°C in the south-central Arabian Sea during the southwest monsoon season relative to other months. Offline computations of the profiles of vertical diffusivity of heat reveal stronger and deeper penetration of heat into the Arabian Sea during the southwest monsoon season. The results presented in the paper demonstrate that the combined effects of strong wind-driven mixing by the monsoonal winds, weak density stratification in the upper-ocean, and downwelling in south-central Arabian Sea, along with strong vertical diffusivity, favor downward transfer of warm waters from the surface into the thermocline. Besides the climatological seasonal cycle, the present study also examines the impact of monsoon interannual variability on the upper-ocean response, by analysis of long-term observed records during (1955–2001) as well as the Argo observations for (2002–2003). It is found that the interannual variations in the ocean response reveal signatures of the influence of strong and weak southwest monsoons on the mixed layer and thermocline variabilities.

Citation: Ramesh, K. V., and R. Krishnan (2005), Coupling of mixed layer processes and thermocline variations in the Arabian Sea, *J. Geophys. Res.*, *110*, C05005, doi:10.1029/2004JC002515.

1. Introduction

[2] Dynamical interactions between the oceanic mixed layer and the underlying thermocline provide vital information about the mechanisms of ocean heat storage [*White et al.*, 1998; *Meehl*, 1984]. The importance of such interactions is examined for the northern Indian Ocean, which exhibits a prominent semi-annual cycle of mixed layer depth variations associated with the seasonally reversing monsoonal circulations [*Düing and Leetmaa*, 1980; *Shetye*, 1986; *Rao et al.*, 1989; *McCreary et al.*, 1993; *Lee et al.*, 2000; *Weller et al.*, 2002]. Moored buoy observations in the Arabian Sea have documented the twice-yearly cycle of mixed layer deepening and cooling during the northeast (winter) and southwest (summer) monsoon seasons [*Weller et al.*, 1998; *Rochford et al.*, 2000; *Prasad and Ikeda*, 2001; *Weller et al.*, 2002]. It is also known that the primary local mechanism driving the mixed layer response is different for the two monsoons. The winter monsoon is characterized by mild dry winds, clear skies, excess evaporation over precipitation, and net heat loss from the ocean, so that the negative buoyancy flux plays a major role in the convective deepening and cooling of the mixed layer. On the other hand, the summer monsoon is characterized by strong southwest monsoon winds, enhanced evaporation from the Arabian Sea, and heavy precipitation along the west coast of India. The strong forcing by the southwest monsoonal winds causes deepening of the mixed layer through shear generation of turbulence and mixing.

[3] Past studies have investigated the roles of various processes in setting up the mixed layer structure of the Arabian Sea during the southwest monsoon season. These include the effects due to upwelling [*Düing and Leetmaa*, 1980; *Schott*, 1983; *McCreary and Kundu*, 1989], wind-driven mixing [*McCreary et al.*, 1993; *Lee et al.*, 2000; *Weller et al.*, 2002], Ekman pumping [*Bauer et al.*, 1991; *McCreary et al.*, 1993], advection of upwelled waters [*Shetye*, 1986; *Molinari et al.*, 1986; *Rochford et al.*, 2000], surface cooling due to evaporation, transport of upwelled waters by mesoscale eddies [*Fischer et al.*, 2002], and so on. Furthermore, recent results from the Arabian Sea Monsoon Experiment (ARMEX) have brought out the formation and evolution of a mini warm pool, with SST greater than 30°C, in the Arabian Sea prior to the onset of the southwest monsoon [*Rao and Sivakumar*, 1999;

[1]Now at CSIR Centre for Mathematical Modeling and Computer Simulation (C-MMACS), Bangalore, India.

0148-0227/05/2004JC002515

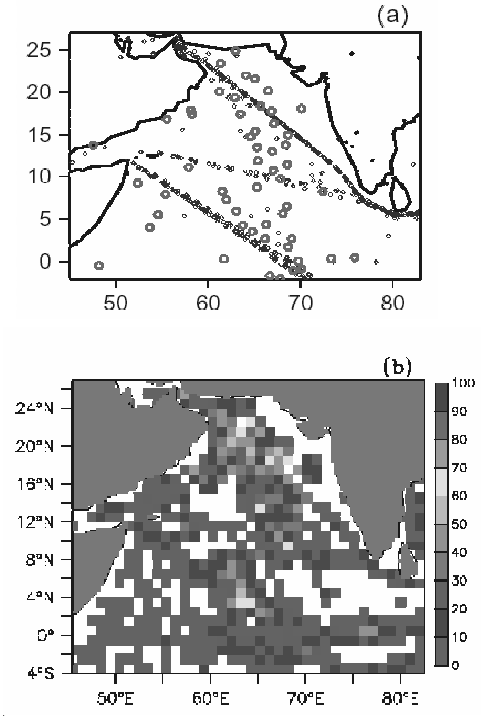

Figure 1. (a) Mean location of Argo floats shown by red circles and measurements from XBT lines and ship cruises shown by blue circles. (b) Number of observations for the period January 2002 to December 2003. The counts are shown on $1^\circ \times 1^\circ$ grid boxes. See color version of this figure in the HTML.

Durand et al., 2004]. *Rao and Sivakumar* [1999] investigated the heat budget of the mixed layer of the Arabian Sea and showed that the heat buildup occurring in the mixed layer during the pre-monsoon months (April and May) is primarily driven by the heat flux through the ocean-atmosphere interface. On the other hand, there are studies which suggest that the formation and development of a barrier layer in the southeastern Arabian Sea (SEAS) plays an important role in the evolution, maintenance, and collapse of the Arabian Sea mini warm pool [*Durand et al.*, 2004; *Shenoi et al.*, 2004]. Results from these studies indicate that the barrier layer forms during the winter season due to advection of low-salinity waters from the Bay of Bengal, which then leads to a marked temperature inversion and contributes to the warming of the mixed layer in the SEAS during the pre-monsoon months. The ARMEX measurements further showed that the barrier layer starts collapsing from April onward. With the arrival of high saline waters from the Arabian Sea and increased upwelling in the SEAS, the barrier layer is annihilated in May [*Shenoi et al.*, 2004].

[4] One of the basic questions is concerning the impact of mixed layer processes on the properties of the thermocline. *Rao and Sivakumar* [2000] examined the seasonal cycle of monthly climatological temperatures for the tropical Indian Ocean. Their results showed that the Arabian Sea SST was cooler by as much as 4°C in August as compared to May. On the other hand, the temperature at 100 m depth in the south-central Arabian Sea was warmer in August by about 3°C relative to May. It was also suggested by *Rao and Sivakumar* [2000] that the seasonal subsurface warming during the northern summer could be associated with downwelling. A key issue, however, that still needs in-depth understanding is about the impact of the southwest monsoonal forcing on the interactions between the waters in and above the thermocline.

[5] The main objective of this study is to understand the role of the southwest monsoon circulation in influencing the Arabian Sea response through physical interactions between the mixed layer and the thermocline underneath. In addition, the study also examines the interannual variability of the upper-ocean temperatures in relation to interannual variations of the southwest monsoon circulation. In order to address these issues, a detailed diagnostic analysis of observed oceanic and atmospheric data sets from multiple sources has been carried out. The paper is organized as follows. The data sources used in the present study along with details regarding the construction of the monthly gridded Argo data for 2002–2003 are described in section 2. The diagnostic analysis, presented in section 3, is divided into subsections: the determination of mixed layer depth, the climatological annual cycle of changes in the upper-ocean temperature, analysis of physical processes associated with the annual cycle, and offline computations of vertical diffusivity of heat in the Arabian Sea. The changes in the upper-ocean response associated with the interannual variability of the southwest monsoon are described in section 4. The results of the study are summarized in section 5.

2. Data Sets

[6] The monthly climatological data sets used for the present study include the following: (1) ocean temperature in the upper 500 m from the World Ocean Atlas (WOA2001) [*Conkright et al.*, 2002] at fixed depth levels (0, 10, 20, 30, 50, 75, 100, 125, 150, 200, 250, 300, 400, 500 m) and (2) climatological air-sea fluxes of heat, momentum, and freshwater from the Southampton Oceanography Centre (SOC) data set [*Josey et al.*, 1999] and climatological mean of ocean currents from the Geophysical Fluid Dynamics Laboratory Assimilation Data set (GFDLAD), which is a 20-year (1981–2000) monthly data set based on a four-dimensional data assimilation [*Derber and Rosati*, 1989] (publicly available from http://data1.gfdl.noaa.gov/nomads/forms/assimilation.html). The air-sea fluxes from the SOC data set are calculated based on marine meteorological reports and validated with independent buoy observations [*Josey et al.*, 1999].

[7] Long-term data of monthly ocean temperatures for the period (1955–2001) from the Joint Environmental Data Archive Center (JEDAC) are used for examining the interannual variability of upper-ocean temperatures. The JEDAC data set, constructed from bathythermograph and hydrographic temperature profiles [*White*, 1995], has temperatures at the following depths (0, 20, 40, 60, 80, 120, 160, 200, 240, 300, 400 m). Additionally, temperature observations from more than 50 Argo floats together with eXpendable BathyThermographs (XBTs) measurements in the Arabian Sea (Figure 1a) for the period (January 2002 to December 2003) are analyzed. The Argo observations were obtained from the Coriolis Center, France (http://www.ifremer.fr/coriolis). A detailed description of the Argo

observing system is given by *Roemmich and Owens* [2000]. The float identification number, number of observations, period of observations, and mean position of the Argo floats used in this study are given in Figure 2. Detailed information about the XBT lines and the data can be obtained from http://www.aoml.noaa.gov/phod/trinanes. A monthly temperature data set has been constructed using the in situ Argo and XBT observations for the period (January 2002 to December 2003), the details of which are described herein. Other data sets used in this study include surface winds from National Center for Environmental Prediction (NCEP) reanalysis data for the period 1955–2003 [*Kalnay et al.*, 1996; *Kistler et al.*, 2001] and surface winds from QuikSCAT [*Pegion et al.*, 2000] for the southwest monsoon seasons of 2002 and 2003.

[8] The in situ temperature observations from the Argo and XBT measurements are used to construct a monthly data set on a ($1^\circ \times 1^\circ$) horizontal grid at fixed vertical depths (0, 10, 20, 30, 50, 75, 100, 125, 150, 200, 250, 300, 400, 500 m) in the upper 500 m for the period (January 2002 to December 2003). First, the temperature observations from the Argo and XBT measurements are collected at fixed depths for a full month. Linear interpolation in the vertical is performed when observations are not available at the above fixed depths. Figure 1b shows the total number of observations on ($1^\circ \times 1^\circ$) grid boxes for the period (January 2002 to December 2003) available for preparing the gridded data set. On an average, there are about 280 observed temperature profiles every month in the Arabian Sea domain. Next, the observations are gridded through an objective analysis procedure which is based on the successive correction method [*Cressman*, 1959], in which the analyzed field at a particular point is given by the sum of a background first-guess field at that point and the weighted mean of corrections (differences between the observed values and the background field) at their respective locations within a specified radius of influence. The analysis is repeated several times with the background field for each iteration being provided by the analyzed field from the previous one and the radius of influence being reduced on each scan to restore information at successively small scales. Every observation within a given scan circle is assigned a weight depending on its distance from the grid point. By defining $X^{a(k)}$ as the value of the analyzed field at a particular location during the kth scan, then the corresponding value in the following scan is given by

$$X^{a(k+1)} = X^{a(k)} + \sum W_j^{k+1}\left(X_j^O - X_j^{a(k)}\right), \qquad (1)$$

where the sum is over all points for which there are observations within a region of influence of radius $R(k)$ about the analyzed point. X_j^O and $X_j^{a(k)}$ are the observed and analyzed values during the kth scan. In the first scan, the background value ($X^{a(0)}$) is given by an appropriate first-guess field. In this case, the monthly climatological temperature from the WOA2001 data set is used as the background first-guess field. The weight function W_j^k at the jth point and kth scan is dependent on the distance (d_j) of each observation from the analyzed point.

$$W_j^k = \frac{R(k)^2 - d_j^2}{R(k)^2 + d_j^2}. \qquad (2)$$

In this study, we use 30 scans (iterations) having radii (600, 580, 560, . . ., 20 km) respectively. This analysis scheme is applied to the temperature field at all the vertical depths, by taking one level at a time. Thus, a three-dimensional gridded monthly data set is prepared taking into account the observations in the Arabian Sea during the period (January 2002 to December 2003). Hereinafter we shall refer to this data set as DINDOCN.

3. Analysis of Mixed Layer and Thermocline Interactions

3.1. Mixed Layer Depth Criterion

[9] The ocean mixed layer depth (MLD) is generally defined as a quasi-homogeneous surface region of density, formed by a history of mixing, that directly interacts with the atmosphere [*Brainerd and Gregg*, 1995]. The study by *Kara et al.* [2003] investigated the spatial and monthly variability of the climatological MLD for the global ocean. The criterion for defining the MLD was based on water density which accounts for the effects of both temperature and salinity. In addition, *Kara et al.* [2003] created a set of isothermal layer depth (ILD) climatologies with different cases of temperature difference (ΔT) criteria. By comparing the ILD with the MLD, they determined an ILD definition that was most nearly equivalent to the optimal MLD [*Levitus and Boyer*, 1994; *Kara et al.*, 2000]. In particular, they demonstrated the validity of the ILD correspondence to MLD using subsurface temperature and salinity data from the Woods Hole Oceanographic Institute (WHOI) mooring deployed in the Arabian Sea. Here we shall consider the results of their analysis for the Arabian Sea, based on the WHOI mooring data from November 1994 to October 1995. Analysis of daily layer depth values obtained by *Kara et al.* [2003] using different (ΔT) values showed that the ILDs with ($\Delta T = 0.8^\circ$C) yielded an optimal MLD in the Arabian Sea. It can be seen from Figure 3a that there is very good agreement between the daily time series of ocean layer depths between MLD (0.8°C) and ILD (0.8°C) in the Arabian Sea. In keeping with the results of *Kara et al.* [2003], we have chosen to define the MLD in the present study to be equivalent to an ILD having a temperature difference of $\Delta T = 0.8^\circ$C. In other words, the MLD is calculated as the depth at which the temperature is 0.8°C below SST. The advantage in using the ILD is that it allows estimation of MLD even in the absence of salinity data. Figure 3b shows the monthly mean values of ILD (0.8°C) at (15.5°N, 61.5°E) in the Arabian Sea for the June–September months during 1995, 2002, and 2003. The monthly values for 1995 are based on the WHOI mooring data. The values for 2002 and 2003 are from the DINDOCN data set. It can be noticed that the ILD values are generally high for the month of July during the southwest monsoon season. There are also significant interannual variations in the ILD associated with the variability of the southwest monsoon. It will be seen later in section 4 that the ILD variations in the Arabian Sea, inferred from the long-term temperature data of JEDAC are useful indicators of mixed layer changes associated with the interannual variability of the southwest monsoon.

3.2. Annual Cycle of Temperature Variations

[10] We first examine the annual cycle of climatological monthly temperatures, from the WOA2001 data set, at

2900233 (31)	**2900229** (42)	**2900230** (42)	**2900193** (50)	**2900080** (147)
28-10-2002 to	04-11-2002 to	06-11-2002 to	01-01-2002 to	02-01-2002 to
26-04-2003	29-12-2003	31-12-2003	22-12-2003	28-12-2003
80.1E, 0.1N	70E, 0.2N	66.1E, 2.2N	70.6E, 7.7N	64.9E, 3.0N
2900085 (120)	**2900087** (44)	**2900088** (111)	**2900086** (40)	**2900089** (124)
18-04-2002 to	18-04-2002 to	18-04-2002 to	18-04-2002 to	19-04-2002 to
29-12-2003	04-12-2002	29-12-2003	14-11-2002	30-12-2003
55.76E, 14.5N	54.9E, 15.1N	60.8E, 17.4N	48.8E, 13.3N	64.4E, 21.8N
2900090 (124)	**2900091** (124)	**2900164** (79)	**2900165** (76)	**2900166** (80)
19-04-2002 to	19-04-2002 to	10-01-2002 to	02-01-2002 to	01-10-2002 to
30-12-2003	30-12-2003	30-12-2003	22-12-2003	31-12-2003
67.8E, 18.2N	66.4E, 14.5N	61.4E, 6.9N	61.7E, 0.6S	62.8E, 3.3N
2900167 (80)	**2900168** (79)	**2900194** (51)	**2900159** (73)	**2900161** (69)
08-01-2002 to	06-01-2002 to	03-08-2002 to	07-01-2002 to	07-01-2002 to
29-12-2003	27-12-2003	26-12-2003	28-12-2003	18-12-2003
62.4E, 6.4N	63.3E, 8.4N	57.1E, 11.0N	64.9E, 12.8N	64.8E, 18.9N
2900162 (69)	**2900163** (74)	**2900235** (29)	**2900101** (37)	**2900210** (25)
08-01-2002 to	08-01-2002 to	07-11-2002 to	12-12-2002 to	01-05-2002 to
29-12-2003	29-12-2003	14-08-2003	26-12-2003	28-05-2002
62.3E, 17.5N	66.9E, 16.6N	65.6E, 3.1S	74.8E, 0.9S	57.9E, 17.3N
2900211 (186)	**2900135** (57)	**2900097** (48)	**2900096** (62)	**2900095** (64)
01-05-2002 to	20-01-2003 to	20-01-2003 to	20-01-2003 to	20-01-2003 to
12-12-2002	01-11-2003	22-09-2003	31-12-2003	31-12-2003
65.8E, 19.1N	61.6E, 23.9N	64.8E, 20.6N	61.4E, 19.9N	66.4E, 17.6N
2900156 (28)	**2900157** (28)	**2900158** (28)	**2900159** (27)	**2900098** (54)
17-03-2003 to	17-03-2003 to	18-03-2003 to	18-03-2003 to	20-01-2003 to
25-12-2003	26-12-2003	26-12-2003	27-12-2003	22-10-2003
62.7E, 5.8N	64.8E, 3.0N	67.0E, 1.8N	68.5E, 1.6S	63.2E, 21.9N
2900134 (65)	**2900259** (42)	**2900260** (43)	**2900256** (40)	**2900258** (41)
20-01-2003 to	04-06-2003 to	03-06-2003 to	05-06-2003 to	07-06-2003 to
31-12-2003	31-12-2003	30-12-2003	27-12-2003	29-12-2003
60.9E, 23.4N	66.8E, 10.2N	67.3E, 9.6N	64.9E, 15.0N	68.7E, 11.5N
2900261 (40)	**2900262** (37)	**2900273** (38)	**2900264** (37)	**2900276** (42)
14-06-2002 to	20-06-2003 to	23-06-2003 to	17-06-2003 to	05-06-2003 to
31-12-2003	27-12-2003	30-12-2003	28-12-2003	27-12-2003
68.6E, 7.4N	67.2E, 4.9N	85.7E, 5N	68.2N, 2.8N	66.6E, 12.5N
2900232 (34)	**1900122** (40)	**2900228** (78)	**2900274** (35)	**2900263** (36)
29-10-2002 to	29-11-2002 to	27-10-2002 to	27-06-2003 to	16-06-2003 to
19-05-2003	24-12-2004	31-12-2003	29-12-2003	28-12-2003
85.98E, 3.683N	78.48E, 4.8S	76.8E, 0.88N	84.1E, 4.6N	69.5E, 5.7N

Figure 2. The WMO float identification number, number of observations (shown in brackets), period of observations, and mean position of the Argo floats used in this study. Floats having fewer than 10 observations, during January 2002 to December 2003, are not shown.

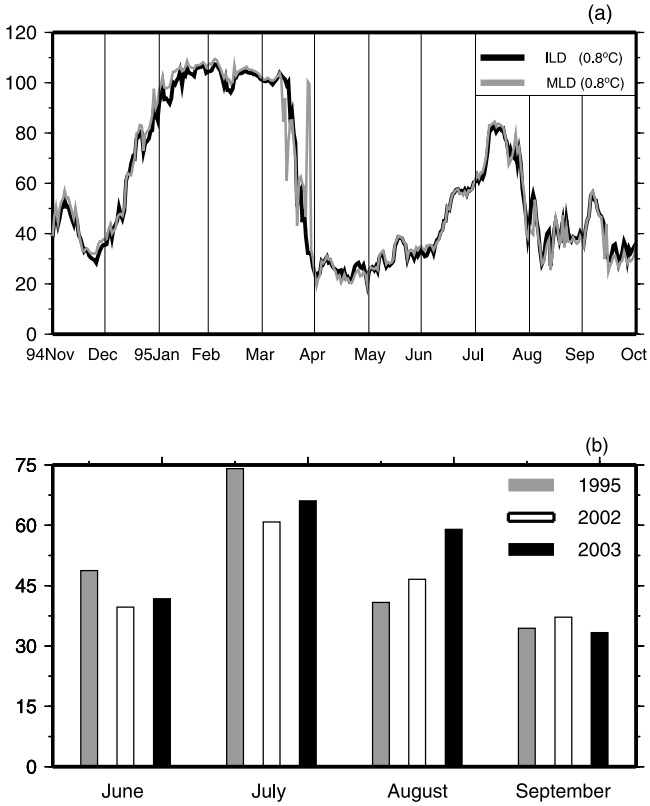

Figure 3. (a) Daily time series of MLD (0.8°C) expressed in meters, from the WHOI mooring in the Arabian Sea (15.5°N, 61.5°E) from November 1994 to October 1995. The MLD and ILD time series are adapted from *Kara et al.* [2003]. (b) Monthly values of ILD (0.8°C) for the southwest monsoon seasons of 1995, 2002, and 2003. The 1995 values are based on the WHOI mooring data in the Arabian Sea; the 2002 and 2003 values are from the DINDOCN data calculated at the WHOI mooring location. See color version of this figure in the HTML.

different depths in the Arabian Sea (Figure 4). It can be noticed that the seasonal cycle of temperature variations in the top 50 m (Figures 4a, 4b, and 4c) is associated with a semi-annual variation characterized by cooling during the winter (December–February) and summer (June–September) monsoon months, but prominent warming in the spring (March–May) and a weak secondary peak in the (October–November) inter-monsoon transition months. The temperature variations in the deeper levels (Figures 4d, 4e, and 4f) exhibit a gradual seasonal warming from January to March, followed by decrease in April and May. The atmospheric conditions during late spring, associated with light winds, clear skies, and intense solar radiation, warms the surface. On the other hand, the mixed layer shoals during late spring as can be seen from Figure 3a, which shows ILD values of about 25 m during April and May. *Weller et al.* [2002] have reported that the shoaling of the mixed layer at this time of the year is within 20 m of the surface and sometimes disappears altogether. An intriguing feature of the subsurface temperature variations is the distinctive warming during the summer monsoon (June–September) season as evident from the temperature maxima in Figures 4d–4f. The peculiarity of this feature is that the seasonal warming in the subsurface during the southwest monsoon months occurs in conjunction with the surface cooling of the Arabian Sea. In an earlier study, *Rao* [1987] examined the upper-ocean thermal response using observations from four stationary ships in the central Arabian Sea during the Monsoon-77 experiment and suggested the possibility of downwelling at the base of the mixed layer during the pre-onset and post-onset phases of the southwest monsoon.

[11] The latitude-depth sections of mean temperature in the northern Indian Ocean for the June–September months, based on the WOA2001 and JEDAC climatological data sets, are shown in Figure 5a and Figure 5b, respectively. The temperatures in the top 50 m, in both the data sets, reveal a sharp decrease from equator to 15°N, while the subsurface temperatures below 80 m show a gradual in-

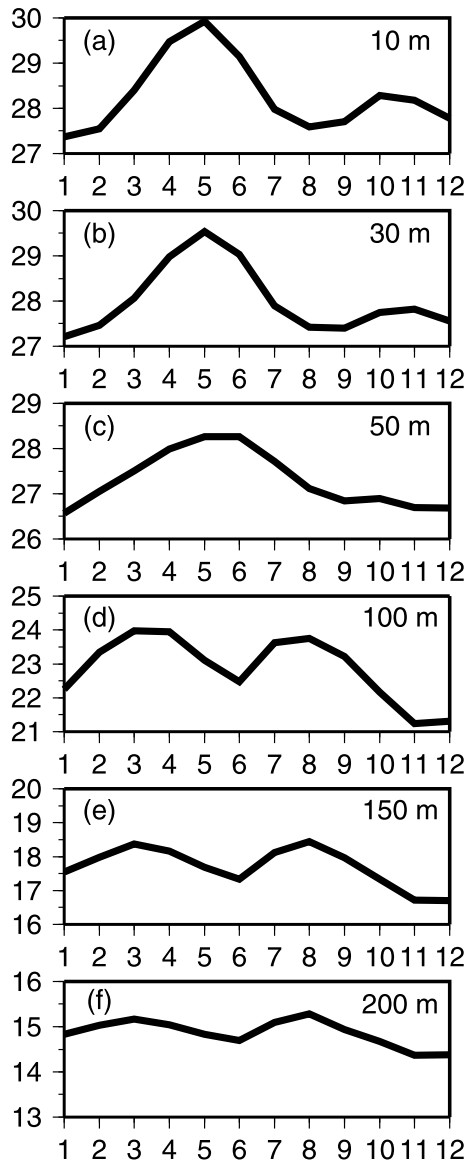

Figure 4. Time series of monthly climatological temperatures (°C) from WOA2001 data set averaged for the region (50°E–70°E; 0°–20°N) at different depths: (a) 10 m, (b) 30 m, (c) 50 m, (d) 100 m, (e) 150 m, and (f) 200 m.

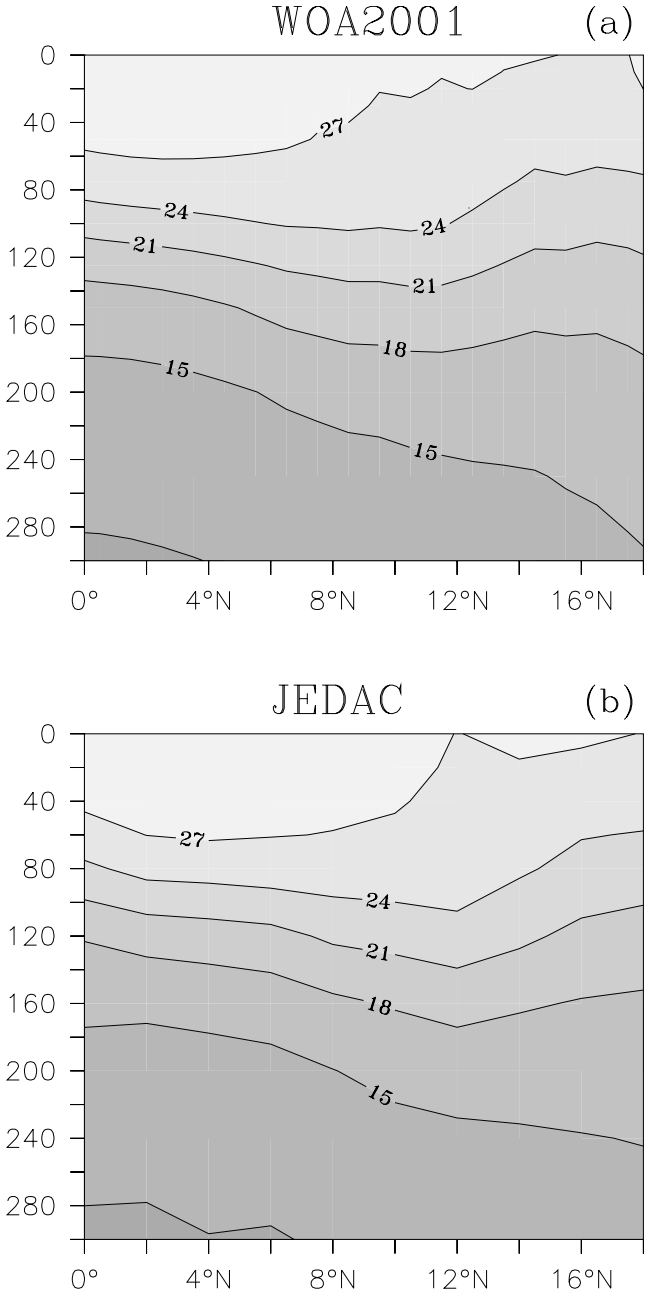

Figure 5. Latitude-depth section of climatological temperature (°C) during June to September, zonally averaged across (50°E–70°E), based on (a) WOA2001 and (b) JEDAC. It may be noted that the JEDAC data are available on a coarser horizontal (5° lon × 2° lat) grid with fewer vertical levels as compared to the WOA2001 data.

crease from equator to about 12°N. In order to better illustrate the thermal response of the Arabian Sea to the southwest monsoon circulation, we contrast the temperature distributions between the summer monsoon season and rest of the year (all months excluding the summer monsoon season). The vertical profiles of temperature, computed from the WOA2001 climatology, for the summer monsoon months (T_{JJAS}) and for rest of the year (T_{REST}) are shown by the solid and dashed lines, respectively, in Figure 6a. The corresponding profiles based on the JEDAC climatology are shown in Figure 6b. The vertical profiles in both the data sets show that the temperature in upper 70 m is about 27.0°C during the southwest monsoon (solid line) and about 27.6°C for the rest of the year (dashed line). The unshaded area between the two curves in Figures 6a and 6b indicates cooling of the mixed layer during the southwest monsoon season by about 0.6°C relative to other months. Model experiments have demonstrated that upwelling and horizontal advection of heat are major processes that contribute to the Arabian Sea cooling during the southwest monsoon season [*Shetye*, 1986; *Molinari et al.*, 1986; *McCreary and Kundu*, 1989].

[12] Another aspect to be noted in Figures 6a and 6b is the temperature gradients, associated with the thermocline, for the T_{JJAS} and T_{REST} profiles. The shaded area in Figures 6a and 6b indicates a relatively warmer thermocline during the southwest monsoon season as compared to other months. The T_{JJAS} and T_{REST} vertical profiles based on the DINDOCN data set are shown in Figure 6c. Clearly, the seasonal differences between T_{JJAS} and T_{REST} are quite robust in indicating the mixed layer cooling and thermocline warming during the southwest monsoon season relative to other months. The upper-ocean thermal response to the monsoonal forcing can be clearly depicted by taking the temperature difference between the southwest monsoon season and the rest of the year. Figure 6d and Figure 6e show the latitude-depth section of the temperature difference between T_{JJAS} and T_{REST} as computed from the WOA2001 and JEDAC data sets, respectively. The latitude-depth sections are based on zonal averages across (50°E–70°E). The pattern of negative values of ($T_{JJAS} - T_{REST}$) extending between equator and 16°N corresponds to the seasonal cooling during the southwest monsoon months, with the maximum cooling exceeding −0.6°C. However, the striking feature in Figures 6d and 6e is the positive pattern of ($T_{JJAS} - T_{REST}$) in the subsurface extending between equator and 14°N, which has a maxima of about 1.2°C near the 150 m depth. The seasonal differences between T_{JJAS} and T_{REST} from the DINDOCN data set (Figure 6f) provides further corroborative evidence for the seasonality of the mixed layer and thermocline responses during the southwest monsoon season as compared to other months.

3.3. Physical Processes Associated With the Annual Cycle

[13] The analysis of physical processes driving the seasonal cycle of upper-ocean temperature variability in the Arabian Sea will be taken up in this section. The monthly climatological values of the oceanic and atmospheric parameters, shown in Figure 7, are useful in interpreting the air-sea interactions in the region. The seasonal variation of net surface heat flux (thick line) and wind stress magnitude (thin line with markings) over the Arabian Sea from the SOC climatology is shown in Figure 7a. The net heat flux variation shows a semi-annual cycle with maxima during the April–May and September–October months; and minima during the December–February and June–July months. On the other hand, the surface wind stress forcing is strong in the southwest monsoon season which enhances the evaporation from the Arabian Sea. Owing to the increased

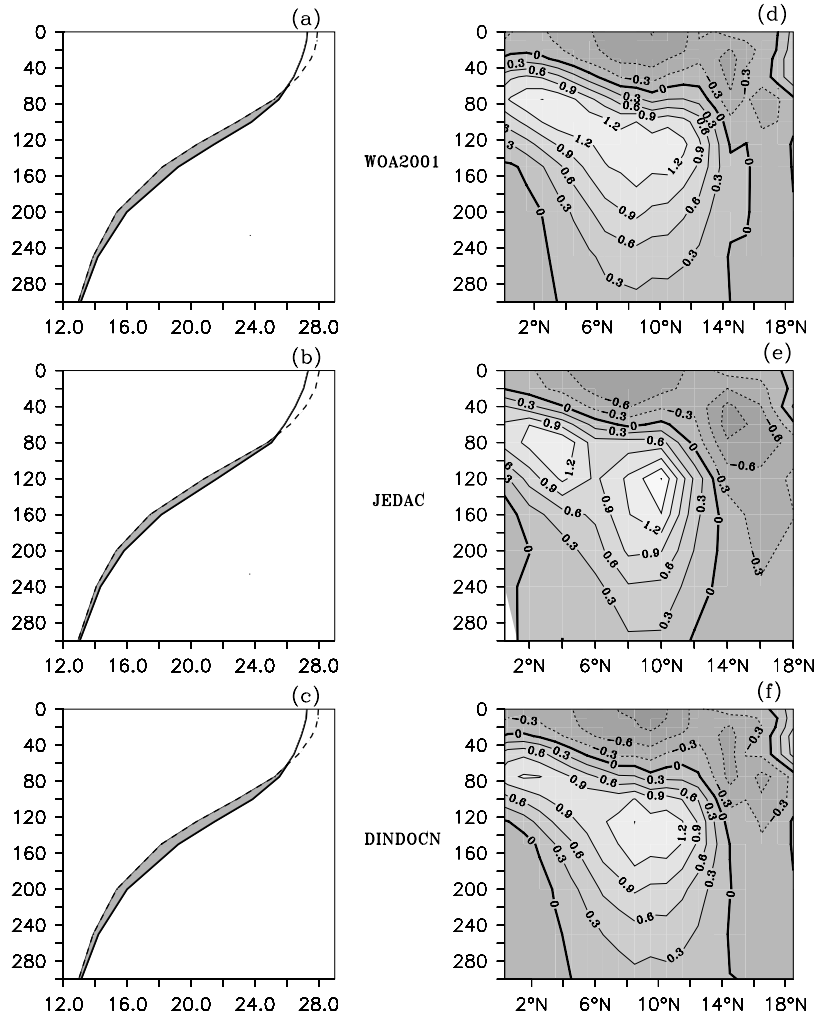

Figure 6. (a) Vertical profile of temperature (°C) averaged for the central Arabian Sea (50°E–70°E; 5°N–15°N) based on the WOA2001 data set. The solid line represents T_{JJAS}, and the dashed line corresponds to T_{REST}. The unshaded region between the two curves shows the area for which T_{JJAS} is less than T_{REST}. The shading shows the area for which T_{JJAS} is more than T_{REST}. (b) Same as Figure 6a except for JEDAC data set. (c) Same as Figure 6a except for DINDOCN data set. (d) Latitude-depth section of the ($T_{JJAS} - T_{REST}$) difference zonally averaged across (50°E–70°E) based on WOA2001. (e) Same as Figure 6d except for JEDAC. (f) Same as Figure 6d except for DINDOCN. See color version of this figure in the HTML.

evaporation, the surface density variation (thick line) in Figure 7b attains a peak during the southwest monsoon season. Further, it can be seen from Figure 7b that the vertical density gradient ($\Delta\rho$) between the surface and the thermocline (thin line with markings in Figure 7b) is minimum in this period. In computing $\Delta\rho$, we have considered the depth of the 20°C isotherm as a reference for the thermocline [*Murthugudde and Busalacchi*, 1999], so that $\Delta\rho$ is calculated by taking the difference between the surface density and the density corresponding to the 20°C isotherm. It can be clearly seen from Figure 7b that the density stratification in the vertical is very weak during the southwest monsoon season. In contrast, the vertical density stratification is strongest during late spring.

[14] The importance of wind-driven mixing in the Arabian Sea during the southwest monsoon season has been pointed out by earlier studies [*McCreary et al.*, 1993; *Lee et al.*, 2000; *Weller et al.*, 2002]. The maxima in the ILD (0.8°C) during July and August in Figure 7c (thick line) is consistent in indicating the deepening of the mixed layer in response to the monsoonal wind forcing. On the other hand, the inter-monsoon transition months are associated with shallow mixed layer. The monthly ILD (0.8°C) averaged for the region (50°E–70°E; 0°–20°N) is about 35 m during April–May and October–November (Figure 7c). The combined effects of the wind stress forcing (Figure 7a) and the density stratification (Figure 7b) can be inferred from the seasonal variation of the Richardson Number ($Ri = \frac{gh\Delta\rho}{\rho_0 u_*^2}$, where $u_* = \sqrt{\frac{\tau}{\rho_0}}$ is the friction velocity and τ is the magnitude of surface wind stress) shown in Figure 7c (thin line with markings). The nondimensional parameter *Ri* is a ratio of the buoyancy forcing versus the rate of production of shear turbulent kinetic energy. It can be noticed from Figure 7c that *Ri* drops to a minimum value lower than 0.25 (critical

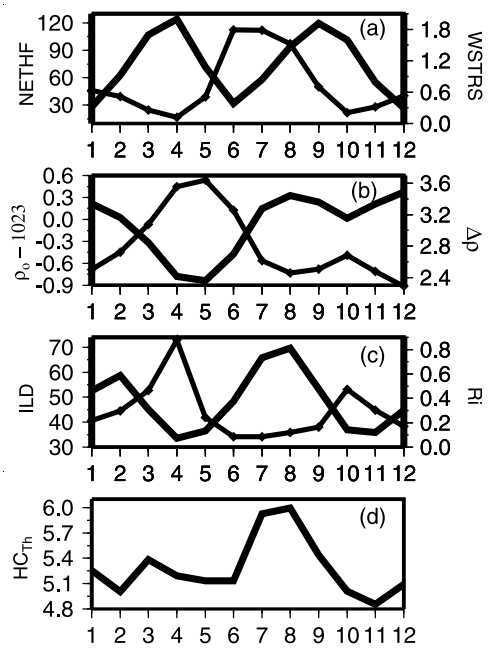

Figure 7. Monthly time series of atmospheric and oceanic parameters averaged for the region (50°E–70°E; 0°–20°N). (a) Net-heat flux (thick line) in W m^{-2} and magnitude of surface wind stress (thin line with markings) in dynes cm^{-2}. (b) Surface density in kg m^{-3} (thick line) after subtracting a reference value of 1023 kg m^{-3}; density difference ($\Delta\rho$) in kg m^{-3} between surface and 20° isotherm (thin line with markings). The density values are computed using the temperature and salinity data from the WOA2001 data set based on the standard UNESCO International Equation of State. (c) ILD (0.8°C) in meters is shown by thick line, and Richardson Number ($Ri = \frac{g h \Delta\rho}{\rho_0 u_z^2}$) is shown by thin line with markings. (d) Heat storage in the thermocline (HC_{Th}) in Joules m^{-3}. See color version of this figure in the HTML.

value for shear instability) during the southwest monsoon season, indicating the unstable structure of the upper ocean. In the subsequent discussions, it will be seen that the strong monsoonal wind-driven mixing is accompanied by strong vertical diffusion of heat from the mixed layer into the thermocline.

[15] A quantitative measure of the seasonal warming of the thermocline during the southwest monsoon months can be obtained by computing the seasonal cycle of heat storage in the thermocline. The magnitude of heat storage in the thermocline (HC_{Th}) can be estimated by taking the difference between the heat content in the upper 300 m of the ocean and the heat content of the mixed layer. As mentioned before, MLD is calculated as the depth at which the temperature is 0.8°C below SST. It can be noted from the equation below that HC_{Th} is a measure of heat storage in the thermocline expressed in Joules m^{-3}.

$$HC_{Th} = \frac{\rho_0 C_p}{(300 - MLD)} \left(\int_{z=0}^{300} Tdz - \int_{z=0}^{MLD} Tdz \right). \quad (3)$$

A similar approach for computing the heat storage has been adopted by *White et al.* [1998]. In the above equation, ρ_0 = 1025 kg m^{-3} is the reference density and C_p = 3994 J $kg^{-1}K^{-1}$ is the specific heat capacity of seawater. The seasonal variation of HC_{Th} averaged for the Arabian Sea (50°E–70°E; 0°–20°N) is shown in Figure 7d. Clearly, it can seen that HC_{Th} attains a maximum value of about 6.0 × 10^{10} Joules m^{-3} during July and August months. The value of HC_{Th} averaged from June to September is around 5.74 × 10^{10} Joules m^{-3}, and the value for rest of the year (all months other than the southwest monsoon season) is found to be around 5.11 × 10^{10} Joules m^{-3}. Thus the increase in HC_{Th} by about 0.63 × 10^{10} Joules m^{-3} indicates greater heat storage in the thermocline during the southwest monsoon season as compared to other months. What happens to this excess heat in the thermocline during the southwest monsoon season? One possibility is that it is partly transported by the seasonal southward meridional currents; part of the solar radiation lost from the mixed layer to the underlying thermocline can be regained in other months [*Kara et al.*, 2004]. Further, it must be pointed out that advective effects within and below the mixed layer are dominant in the Arabian Sea and can significantly contribute to the upper-ocean heat budget during the southwest monsoon season [*Fischer et al.*, 2002]. This point is taken up later in section 3.5. Although it is not fully clear at this stage how the seasonal thermocline warming contributes to the overall heat budget, the mechanisms responsible for the subsurface response of the northern Indian Ocean warrant careful consideration.

3.4. Ekman Pumping During the Southwest Monsoon Season

[16] Insight into the dynamics of vertical motions in the Arabian Sea is helpful in interpreting the upper-ocean response to forcing by the southwest monsoon circulation. The climatological surface wind stress and the curl of wind stress for the southwest monsoon season based on the SOC data set are shown in Figure 8a. The cross-equatorial monsoonal flow is associated with negative wind stress curl over a wide region of the south-central Arabian Sea. The wind stress curl is positive off the coasts of Arabia and Somalia. According to the well-known Sverdrup relation, regions of negative wind stress curl in the Northern Hemisphere are associated with convergence of ocean currents, so that the Ekman pumping gives rise to downward vertical velocity. Conversely, regions of positive wind stress curl are associated with divergence of ocean currents, so that the Ekman pumping gives rise to upward vertical velocity. *Bauer et al.* [1991] have emphasized the role of Ekman dynamics in deepening the mixed layer in the central Arabian Sea during the southwest monsoon season. More recently, *Lee et al.* [2000] have pointed out that the magnitude of Ekman pumping was overestimated in Bauer's model because of the neglect of the latitudinal variation of Coriolis frequency. Following *Lee et al.* [2000], we have computed the vertical velocity due to Ekman pumping (W_{EP}),

$$W_{EP} = \frac{1}{f\rho_0} \left(\hat{k} \cdot (\nabla \times \vec{\tau}) + \frac{\beta}{f} \tau^x \right), \quad (4)$$

where $\vec{\tau} = (\tau^x, \tau^y)$ is the surface windstress, ρ_0 is the reference density, f is the Coriolis frequency, and β is the

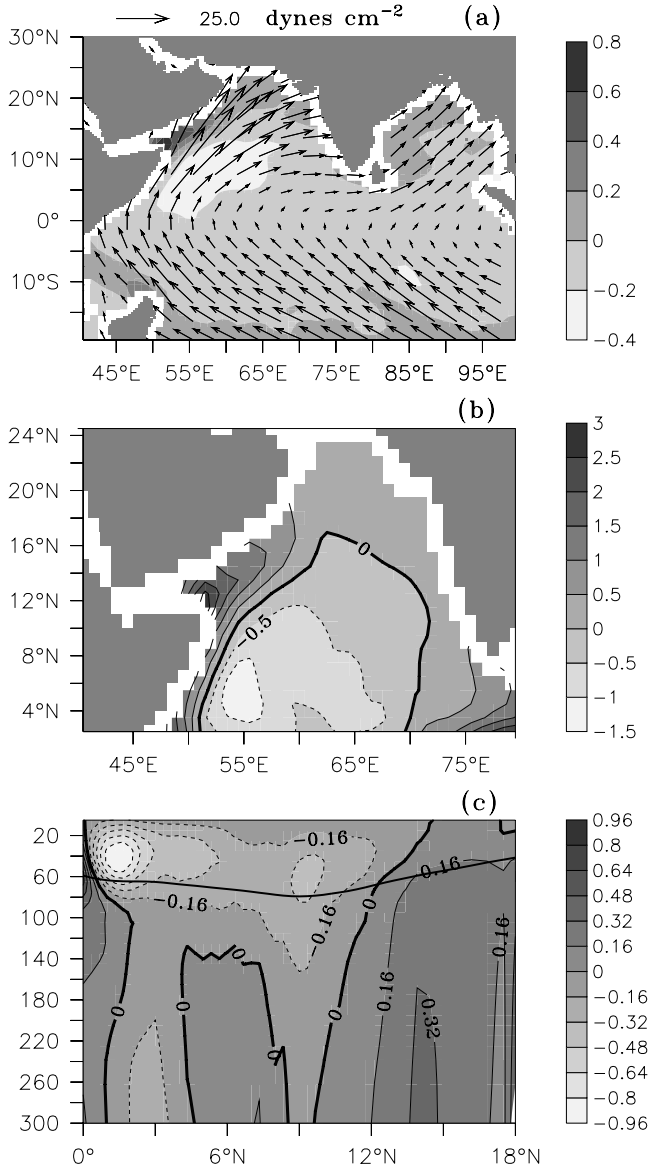

Figure 8. Climatological distribution for the June–September months. (a) Surface wind stress (dynes cm^{-2}) based on SOC data set. The shading represents curl of wind stress (dynes cm^{-1}), and the values have been scaled by a factor of $1.0 \times 10^{+7}$. (b) Ekman pumping vertical velocity (W_{EP}) in cm s^{-1}. (c) Latitude-depth section of the vertical velocity (cm s^{-1}) zonally averaged across (50°E–70°E) based on GFDLAD climatology. The solid line is the zonally averaged ILD (0.8°C) from GFDLAD climatology. The vertical velocities in Figures 8b and 8c are scaled by a factor of 1000. See color version of this figure in the HTML.

latitudinal variation of Coriolis frequency. The climatological Ekman pumping vertical velocity during the southwest monsoon season is shown in Figure 8b. The negative values of W_{EP} in the south-central Arabian Sea indicate downwelling with maximum of about -1.0×10^{-3} cm s^{-1} around (55°E; 5°N). The value of W_{EP} averaged for the Arabian Sea domain (50°E–70°E; 1°N–20°N) is found to be -1.1×10^{-4} cm s^{-1}. Note that the calculation of W_{EP} involves division by the Coriolis frequency, which is zero at the equator. For this purpose, we consider the latitudinal averaging of W_{EP} between 1°N and 20°N. The positive values of W_{EP} off the coasts of Arabia and Somalia indicate coastal upwelling. The magnitude of upwelling due to Ekman divergence averaged for the region (47°E–52°E; 1°N–20°N) is found to be 1.3×10^{-3} cm s^{-1}. The y-z section of climatological vertical velocity from the GFDLAD data set (Figure 8c) is used to illustrate the vertical motions during the southwest monsoon season. The solid line superposed in Figure 8c shows the latitudinal variation of ILD (0.8°C). The predominant feature in Figure 8c is the downward vertical velocity to the south of 12°N in the south-central Arabian Sea. The maximum value of downwelling, in the mixed layer of the near-equatorial region, is about -0.8×10^{-3} cm s^{-1}. The vertical velocity at the base of the mixed layer is around -0.3×10^{-3} cm s^{-1}, and downward velocities can be noticed below the mixed layer. To the north of 13°N, the vertical velocity is positive (upward motion), which corresponds to upwelling in the region of the Gulf of Cambay, the Omani coast, and adjoining area.

3.5. Advection Within and Below the Mixed Layer

[17] Advection within and below the mixed layer is substantial in the Arabian Sea during the southwest monsoon season in association with the strong forcing by the monsoonal winds [*Fischer et al.*, 2002]. Figure 9 shows the horizontal advection terms computed using the climatological mean of ocean currents and temperature from the GFDLAD data set for the southwest monsoon season. The advection terms given below are computed separately for the mixed layer and the thermocline by vertically averaging over their respective depths. The depth of the 20°C isotherm (ISO20) is chosen as reference for the thermocline.

$$ADV_{(MLD)} = \frac{1}{MLD}\int_{z=0}^{MLD} \vec{V} \cdot \nabla T dz, \tag{5}$$

$$ADV_{(Th)} = \frac{1}{(ISO20 - MLD)} TERM, \tag{6}$$

$$TERM = \left[\int_{z=0}^{ISO20} \vec{V} \cdot \nabla T dz - \int_{z=0}^{MLD} \vec{V} \cdot \nabla T dz\right]. \tag{7}$$

The positive values of zonal advection of temperature which extend from the Somali region to the central Arabian Sea, both in the mixed layer and thermocline (Figures 9a and 9c), indicate eastward advection. On the other hand, the negative values of the meridional advection terms (Figures 9b and 9d) correspond to southward advection. It may be noticed that the magnitudes of the zonal and meridional advection terms in the thermocline are relatively larger than those in the mixed layer. Further, it can be seen that the large negative values of meridional advection in the near-equatorial region in Figure 9d are suggestive of strong cross-equatorial

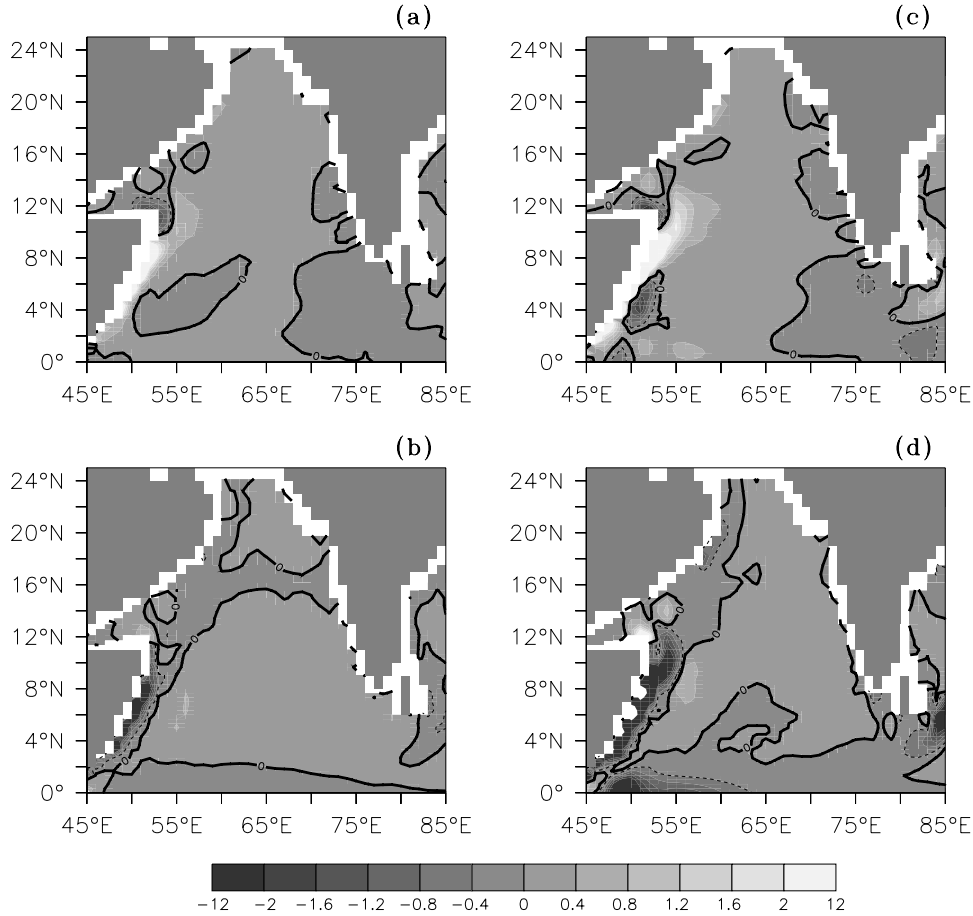

Figure 9. Climatological distribution of temperature advection terms for the June–September months based on the GFDLAD data set. (a) Zonal advection term vertically averaged over the mixed layer depth (unit K s^{-1}). (b) Meridional advection term vertically averaged over the mixed layer depth (unit K s^{-1}). (c) Same as Figure 9a except for thermocline depth. (d) Same as Figure 9b except for thermocline depth. The advection terms have been scaled by a factor of 10,000. See color version of this figure in the HTML.

transport in the thermocline. The term $\rho_0 C_p \times ADV_{(MLD)}$ provides a quantitative measure of the effect of advection on the heat budget of the mixed layer [*Large et al.*, 1986]. The zonal component of $\rho_0 C_p \times ADV_{(MLD)}$ averaged for the Arabian Sea domain (50°E–70°E; 0°–20°N) is found to be about +43 J s^{-1} m^{-3}. It may be noted that the eastward advection of the upwelled waters from the Somali region basically contributes to the mixed layer cooling of the Arabian Sea during the southwest monsoon season. The value of the corresponding term for the meridional component of $\rho_0 C_p \times ADV_{(MLD)}$ is about −9 J s^{-1} m^{-3}. Likewise, we have evaluated the term $\rho_0 C_p \times ADV_{(Th)}$ to determine the advective effects in the thermocline. It is found that the zonal component of $\rho_0 C_p \times ADV_{(Th)}$ averaged for the Arabian Sea domain is about +52 J s^{-1} m^{-3}. On the other hand, the area averaged value of the meridional component of $\rho_0 C_p \times ADV_{(Th)}$ is found to be about −106 J s^{-1} m^{-3}, which significantly contributes to the removal of excess heat in the thermocline. From the above discussions, it is clear that the horizontal advection terms are associated with substantial southward and eastward transport of heat, both in the mixed layer and the thermocline, during the southwest monsoon season which are significant for the upper ocean heat budget of the Arabian Sea.

3.6. Vertical Diffusivity of Heat

[18] Vertical mixing processes in the upper ocean play a key role in determining the exchanges between the mixed layer and the underlying thermocline. *Large et al.* [1994] have provided a detailed review on oceanic vertical mixing processes that operate on a range of time and space scales of importance to climate. They discussed two distinct regimes: ocean mixing in the boundary layer near the surface under a variety of surface forcing conditions (stabilizing, destabilizing, and wind driven) and mixing in the ocean interior due to internal waves, shear instability, and double diffusion (arising from the different molecular diffusion rates of heat and salt).

[19] We have performed offline computations of vertical diffusivity of heat using a one-dimensional model based on the K-Profile parameterization (KPP) scheme [*Large et al.*, 1994, 1997]. The KPP scheme includes vigorous mixing within the turbulent surface boundary layer and relatively weak diapycnal mixing in the ocean interior. The determination of the oceanic boundary layer depth involves param-

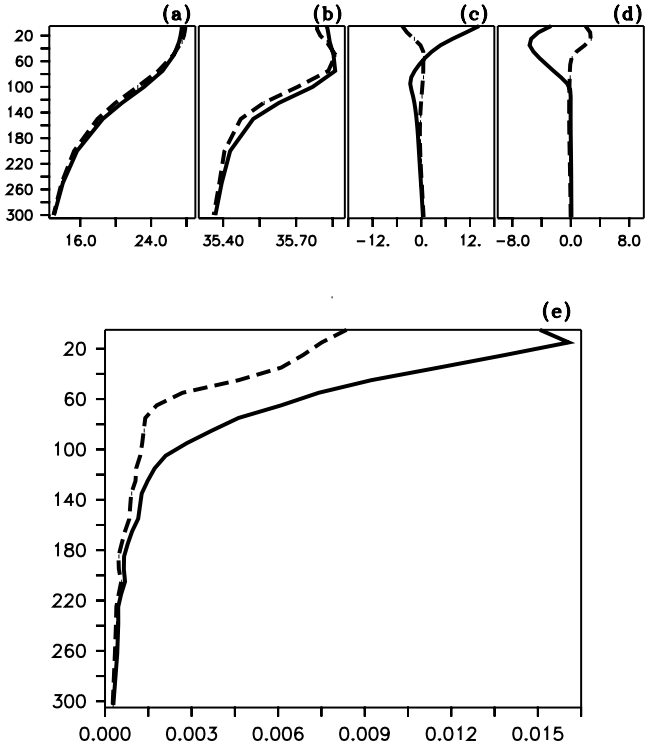

Figure 10. Climatological vertical profiles averaged for the region (50°E–70°E; 0°–20°N). (a) Temperature (°C). (b) Salinity (psu). (c) Zonal velocity (cm s^{-1}). (d) Meridional velocity (cm s^{-1}). (e) Diffusivity of heat (m^2 s^{-1}) computed from the KPP model. The solid lines correspond to the southwest monsoon season (JJAS); the dashed lines correspond to rest of the year (REST). The temperature and salinity profiles are based on the WOA2001 data set; the zonal and meridional currents are from GFDLAD. For the diffusivity calculation, the monthly values of attenuation of photosynthetically available radiation (k_{PAR}) for the Arabian Sea are used for specifying the optical water type in the KPP model as described by *Rochford et al.* [2001].

eterization of the turbulent shear in terms of the bulk Richardson number. An important feature of the KPP scheme is the capability of the boundary layer to penetrate well into a stable thermocline in both convective and wind-driven situations [*Large et al.*, 1994]. For the offline diffusivity calculations, monthly climatological profiles of ocean temperature, salinity, and zonal and meridional velocities, along with forcing of surface fluxes (zonal and meridional momentum fluxes, shortwave flux, sensible heat flux, longwave flux, latent heat flux, and precipitation rate), are provided as input at every 1° × 1° longitude-latitude grid point in the Arabian Sea domain (50°E–70°E; 0°–20°N). The climatological temperature and salinity profiles are based on the WOA2001 data set; the profiles of zonal and meridional velocities are based on the GFDLAD data set; the surface forcing parameters are from the SOC data set. The constant parameters used in the KPP model are (1) critical Richardson number for boundary layer depth = 0.25, (2) Richardson number limit for shear instability = 0.8, (3) maximum viscosity due to shear instability = 0.005 m^2 s^{-1}, (4) maximum diffusion due to shear instability = 0.005 m^2 s^{-1}, (5) background/internal wave viscosity = 0.0001 m^2 s^{-1}, (6) background/internal wave diffusion = 0.00001 m^2 s^{-1}, and (7) salt fingering diffusion factor = 0.001 m^2 s^{-1}. The KPP scheme also takes into account the distribution of solar irradiance in the water column. The depth of penetration of solar radiation is a function of the water clarity (for details see Figure 10).

[20] Table 1 provides information about monthly climatological surface forcing parameters averaged over the Arabian Sea domain. Likewise, the area-averaged vertical profiles of temperature, salinity, zonal velocity, and meridional velocity are illustrated in Figures 10a–10d. The solid lines correspond to profiles for the southwest monsoon season, and the dashed lines correspond to profiles for all other months (excluding June to September). It is clear from Figures 10c and 10d that the velocity profiles in the Arabian Sea indicate strong seasonal changes. Profiles of vertical diffusivity of heat (ν_θ) are computed using the KPP model, for every month, at each grid point in the Arabian Sea domain, and the area-averaged profiles are shown in Figure 10e. It can be seen that the values of ν_θ computed for the southwest monsoon season (solid line) are in the range of (0.0027–0.015) m^2 s^{-1} in the upper 100 m. In the interior, ν_θ varies in the range of (0.0007–0.0027) m^2 s^{-1} between 100 and 200 m, and attains low values farther below. Similar vertical diffusivities ($\geq$0.001 m^2 s^{-1} at the base of the mixed layer; and about 0.0004 m^2 s^{-1} in the thermocline) have been estimated in the northeast Pacific in response to strong autumnal forcing [*Large et al.*, 1986]. Further, it can be seen from Figure 10e that ν_θ values for rest of the year (dashed line) vary roughly between 0.0025 and 0.008 m^2 s^{-1} in the top 60 m, decrease sharply between 60 and 200 m, and attain low values farther below. Thus the vertical diffusivity of heat is not only stronger but also penetrates deeper into the ocean during the southwest monsoon season as compared to other months. The stronger and deeper vertical diffusivity during the southwest monsoon season enables downward transfer of heat from the surface into the thermocline. The above results indicate that the strong monsoonal wind-driven mixing and deep diffusivity of heat is a plausible mechanism that couples the mixed layer and the thermocline, and thus provides a consistent explanation for the warming of the thermocline in the central Arabian Sea during the southwest monsoon season.

4. Response to Monsoon Interannual Variability

[21] Interannual variations in the upper-ocean response associated with the variability of the southwest monsoon are examined using the long-term (1955–2001) monthly ocean temperature data from JEDAC. The climatological ILD (0.8°C) and surface winds for the month of July during the southwest monsoon are shown in Figure 11a. The surface winds are based on the NCEP reanalysis data set. It can be seen that ILD values exceeding 50 m are colocated in the region of strong monsoonal winds between 50°E–70°E and 4°N–14°N. To the north of 15°N, the ILD is less than 40 m. In order to examine the interannual changes in the ocean response, we have constructed composites of ocean temperature anomalies for strong and weak monsoons

Table 1. Monthly Climatological Surface Forcing Parameters Used for Computing the KPP Diffusivity Profiles[a]

	τ_x, N/m^2	τ_y, N/m^2	Shortwave Flux, W/m^2	Longwave Flux, W/m^2	Sensible Heat Flux, W/m^2	Evaporation Rate, kg m^{-2} s^{-1}	Rainfall Rate, kg m^{-2} s^{-1}
Jan.	−0.0377	−0.0506	214.4	−55.49	−4.566	−5.151E-05	1.331E-05
Feb.	−0.0336	−0.0379	248.7	−58.39	−5.114	−5.007E-05	6.525E-06
March	−0.0178	−0.0171	275.2	57.90	−4.069	−4.340E-05	9.124E-06
April	−0.0041	−0.0064	283.5	−56.26	−4.680	−4.013E-05	1.291E-05
May	0.0403	0.0235	251.4	−49.01	−5.253	−5.110E-05	4.104E-05
June	0.1365	0.1051	227.8	−43.48	−1.444	−6.155E-05	3.245E-05
July	0.1245	0.1194	235.1	−45.31	−0.698	−5.355E-05	1.819E-05
Aug.	0.1038	0.1028	247.7	−44.84	0.559	−4.470E-05	1.709E-05
Sept.	0.0458	0.0436	259.7	−48.83	−1.690	−3.656E-05	1.474E-05
Oct.	0.0127	−0.0006	251.8	−53.99	−3.663	−3.787E-05	2.214E-05
Nov.	−0.0111	−0.0222	222.8	−53.85	−4.250	−4.485E-05	2.408E-05
Dec.	−0.0317	−0.0421	209.4	−55.40	−4.577	−4.998E-05	2.822E-05

[a]Values are averages for the Arabian Sea domain (50°E–70°E; 0°–20°N). Read 5.151E-05 as 5.151 × 10^{-5}.

by selecting five strong monsoon cases (1956, 1959, 1961, 1988, 1994) and five weak monsoon cases (1972, 1979, 1982, 1986, 1987). (Dry (wet) monsoons correspond to cases for which the All India Summer Monsoon Rainfall (AISMR) during June to September is less (more) than 90% (110%) of the climatological normal. The AISMR is an area averaged rainfall index based on a fixed set of 306 uniformly distributed raingauge stations [*Parthasarathy et al.*, 1995]. The AISMR data can be obtained from http://www.tropmet.res.in.) The above five weak monsoons actually correspond to years of monsoon drought over India. Conversely, the five strong monsoons are years of excess monsoon precipitation over India. The anomaly composite of surface wind and ILD (0.8°C) based on the strong monsoon events is shown in Figure 11b. In order to focus on the interannual changes in the ocean response, the

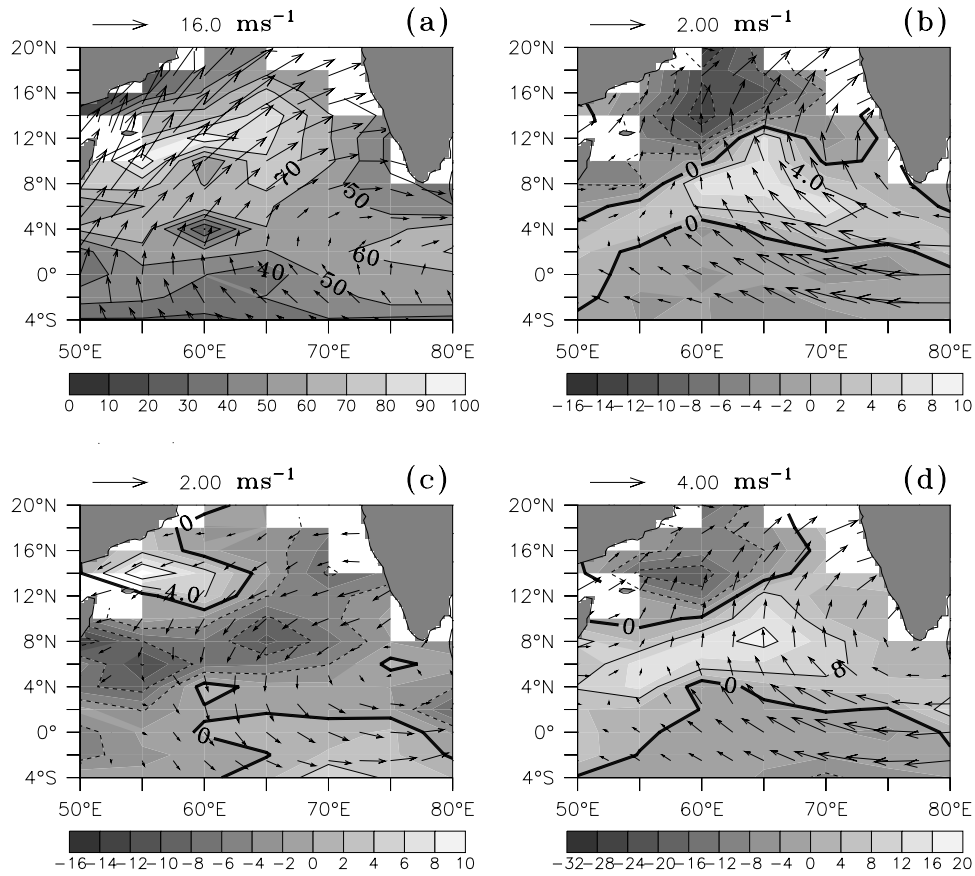

Figure 11. (a) Climatological ILD (0.8°C) in meters and surface winds (m s^{-1}) during July. The ILD is computed using the JEDAC temperature data, and surface winds are from NCEP reanalysis. (b) Strong monsoon anomaly composite of ILD and surface winds. (c) Weak monsoon anomaly composite of ILD and surface winds. (d) Strong minus weak monsoon anomaly composite of ILD and surface winds. See color version of this figure in the HTML.

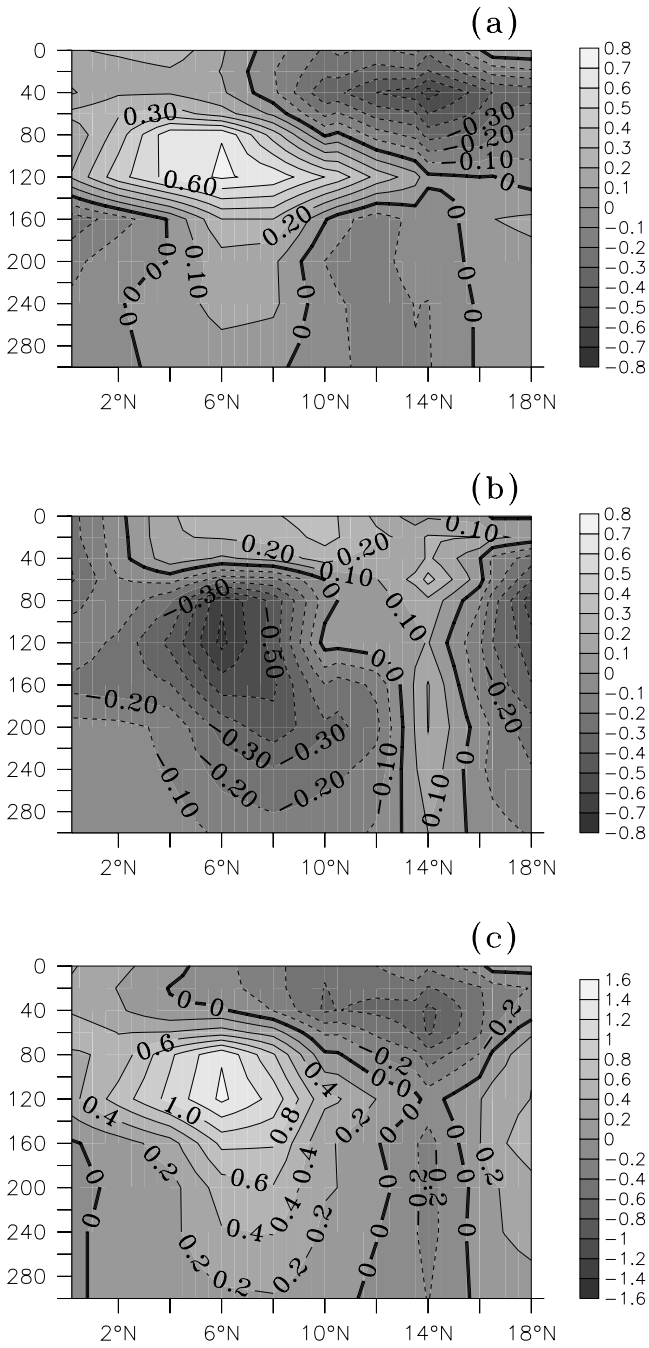

Figure 12. Latitude-depth sections showing temperature (°C) anomalies for (a) strong monsoon composite, (b) weak monsoon composite, and (c) strong minus weak monsoon composite. The temperature anomalies are zonally averaged across (50°E–70°E). See color version of this figure in the HTML.

anomaly composites are shown for the month of July during the southwest monsoon season. By so doing, we actually exclude much of the effects due to subseasonal variability. The strong monsoon composite is consistent in showing an intensification of the cross-equatorial monsoon flow. The increase in the southerly flow across the equator (Figure 11b) is accompanied by anomalous easterlies to the south of the equator and anomalous westerlies to the north of 10°N giving rise to an anomalous anti-cyclonic circulation over the central Arabian Sea. The anomaly composite of ILD (0.8°C) in Figure 11b shows deepening of the mixed layer by as much as 6–8 m, which is a significant variation from the climatology (Figure 11a). The ILD increase is seen mostly in the south-central Arabian Sea; while the ILD anomaly in the northern Arabian Sea is negative. The anomaly pattern for the weak monsoon composite (Figure 11c) is more or less opposite to that of the strong monsoon composite. The low-level wind anomalies in Figure 11c clearly indicate weakening of the monsoon cross-equatorial flow. The ILD is shallower than normal as can be seen from the negative anomalies in the south-central Arabian Sea in Figure 11c. On the other hand, the ILD anomalies show deepening to the north of 12°N. Thus the ILD increase (decrease) in the south-central Arabian Sea in Figure 11b (Figure 11c) is consistent with the strengthening (weakening) of the cross-equatorial monsoon flow. In fact, the strong minus weak monsoon composite (Figure 11d) brings out the range in the ILD changes associated with the monsoon interannual variability.

[22] The upper-ocean temperature changes associated with the strong and weak monsoons are shown by the latitude-depth sections of anomaly composites zonally averaged across (50°E–70°E) in Figure 12a and Figure 12b, respectively. The strong monsoon composite shows anomalous cooling in the upper 80 m. The cooling is mostly seen to the north of 6°N, and the maximum cooling is about −0.5°C. This is consistent with the results of *Joseph and Pillai* [1984] which indicated anomalous cooling (warming) of Arabian Sea SST during years of strong (weak) southwest monsoons. Another remarkable feature in Figure 12a is the anomalous subsurface warming with maximum of about 0.7°C at a depth of about 120 m. The warm subsurface anomaly is prominently seen between the equator and 12°N and extends vertically to a depth of about 250 m. On the other hand, the weak monsoon composite (Figure 12b) shows anomalous warming in the top 50 m and cold subsurface anomalies between the equator and 12°N. The effect of decreased upwelling in the northern Arabian Sea can be inferred from the warm subsurface anomalies in Figure 12b. The strong minus weak monsoon composite (Figure 12c) illustrates the range of temperature changes associated with the monsoon interannual variability. The cold anomalies in the northern Arabian Sea are consistent with enhanced upwelling in the region associated with the monsoon interannual variability, while the warm subsurface anomalies in the south-central Arabian Sea indicate increased downwelling and deeper vertical diffusivity of heat.

[23] The DINDOCN data set (based on the Argo and XBT observations) used in this study has data coverage for the two summer monsoon seasons of 2002 and 2003 and serves as a supplementary data source for examining the Arabian Sea response to monsoon interannual variability. The southwest monsoon circulation was abnormally weak during 2002, and the Indian subcontinent experienced a major monsoon drought [*Gadgil et al.*, 2002]. In particular, extreme dry conditions and anomalously weak monsoon flow patterns led to a major decrease of monsoon rainfall over India in the month of July 2002. Conversely, the southwest monsoon circulation was moderately active dur-

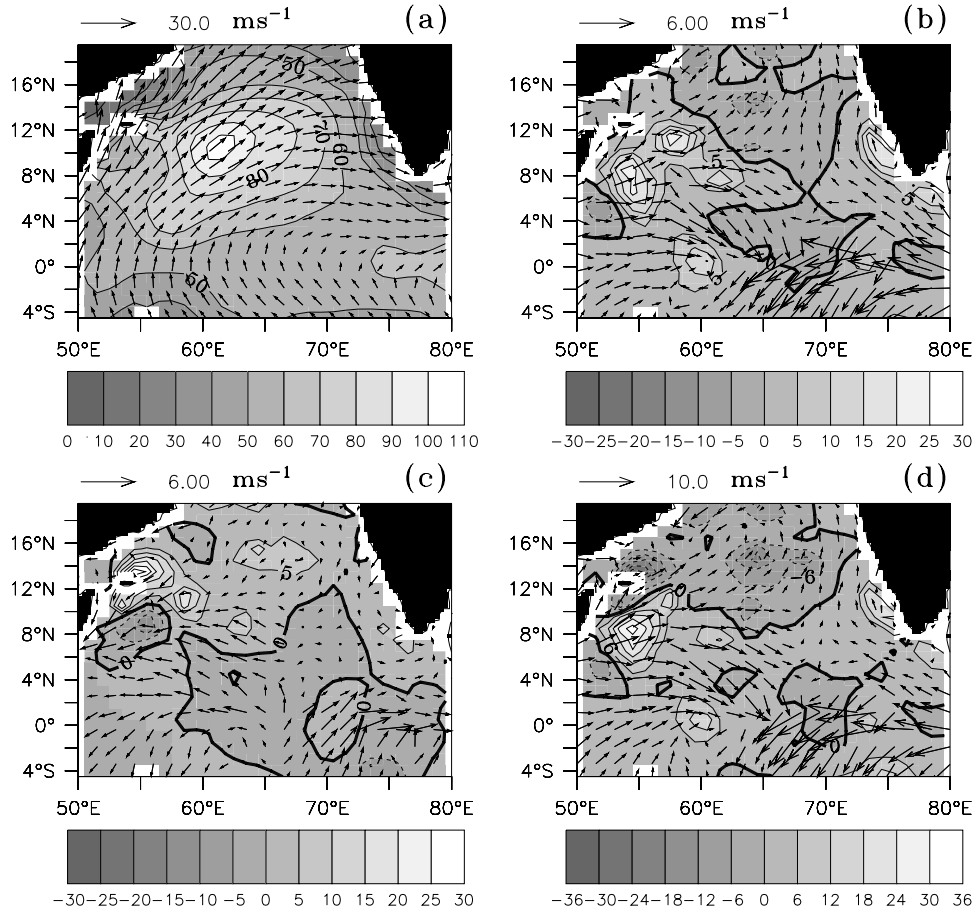

Figure 13. (a) Climatological ILD (0.8°C) in meters and surface winds (m s^{-1}) during July, based on the WOA2001 and QuikSCAT data sets, respectively. (b) Anomalies of ILD and surface winds for July 2003. (c) Anomalies of ILD and surface winds for July 2002. (d) ILD difference and surface wind difference (July 2003 minus July 2002). The ILD anomalies for 2002 and 2003 are computed from the DINDOCN data set relative to the WOA2001 climatology. Note that the DINDOCN data set is constructed from the Argo and XBT observations for 2002 and 2003, and the objective analysis procedure modifies the WOA2001 climatological first-guess field using the Argo and XBT observations. See color version of this figure in the HTML.

ing 2003 which resulted in above normal rainfall over most parts of India. Here we shall compare the oceanic responses between July 2002 and July 2003, because the signal associated with the monsoon interannual variability was dominant for these two months. The climatological ILD (0.8°C) and surface winds during July, based on the WOA2001 and QuikSCAT data sets, are shown in Figure 13a. The correspondence between the region of strong monsoonal winds and the ILD maxima in the central Arabian Sea can be clearly noted in Figure 13a. The ILD anomalies for July 2003 (Figure 13b) indicate an increase in the mixed layer depth in the west-central Arabian Sea to the south of 12°N, and the wind anomalies over this region show intensification of the westerly flow. Furthermore, it may be noted that the easterly wind anomalies extending to the south of the equator in Figure 13b are consistent with a stronger monsoonal flow during July 2003. Also seen in Figure 13b is the decrease in ILD in the northern Arabian Sea associated with the cyclonic circulation anomaly prevailing over the region. On the other hand, the wind anomalies for July 2002 (Figure 13c) show anomalous easterlies over the west-central Arabian Sea corresponding to the weak monsoon circulation. It may also be noticed that the anomalous westerlies east of 68°E and extending south of the equator in Figure 13c correspond to weakening of the monsoon cross-equatorial flow during July 2002. The ILD anomalies for July 2002 reveal a decrease in the mixed layer depth in the south-central Arabian Sea to the south of 8°N, while the ILD anomalies in the northern Arabian Sea show deepening of the mixed layer during July 2002. It a broad sense, it may be inferred that the ILD and wind anomalies during July 2002 were nearly opposite to those during July 2003. The contrast between the monsoon circulations of July 2003 and July 2002 can be clearly seen from the plot of surface wind difference (July 2003 minus July 2002) in Figure 13d. The enhancement of the southwest monsoon winds during July 2003 as compared to July 2002 can be noted from the pattern of anomalous westerlies extending from the Somali coast to the central Arabian Sea. Likewise the anomalous easterlies extending to the south of the equator in Figure 13d indicate intensification of the monsoonal flow during July 2003 relative to July 2002. The ILD

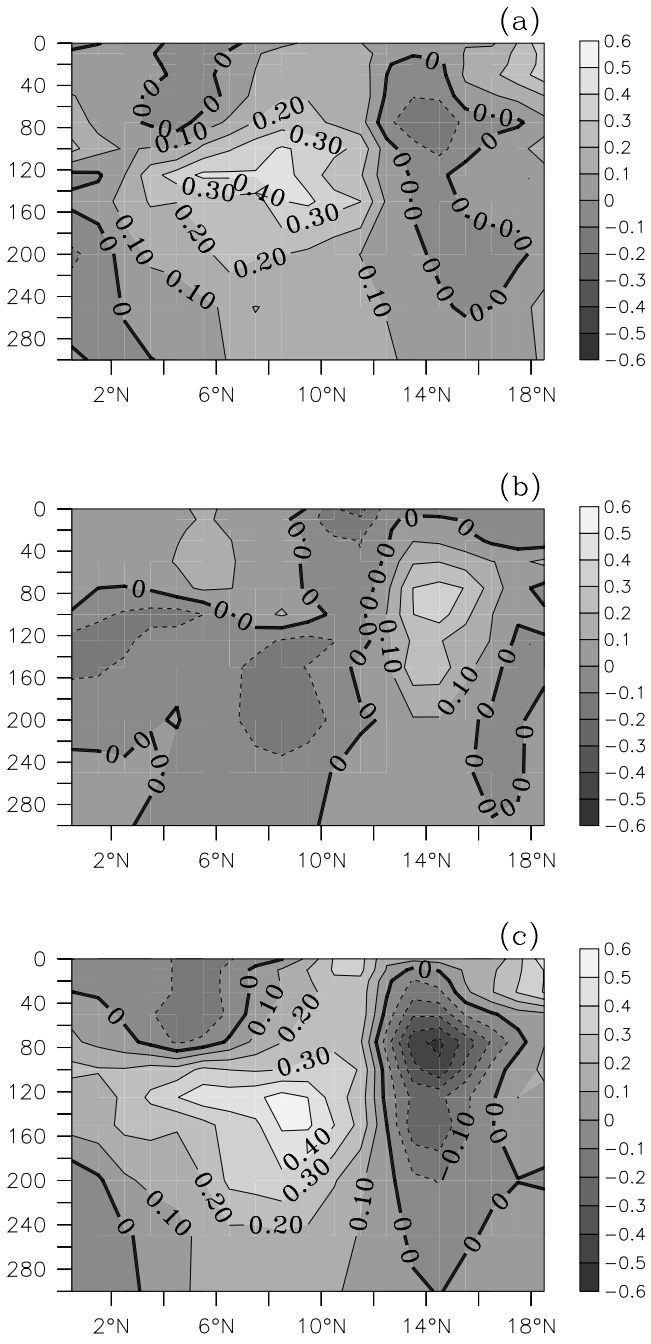

Figure 14. Latitude-depth section temperature (°C) anomalies zonally averaged across (50°E–70°E). (a) July 2003. (b) July 2002. (c) Difference (July 2003 minus July 2002). The temperature anomalies for 2002 and 2003 are based on the DINDOCN data set relative to the WOA2001 climatology. See color version of this figure in the HTML.

anomalies in Figure 13d are consistent with the surface wind anomalies in indicating a deeper mixed layer to the south of 10°N and shallower mixed layer in the northern Arabian Sea during July 2003 as compared to July 2002.

[24] The latitude-depth section of temperature anomalies during July 2003 zonally averaged across the Arabian Sea domain is shown in Figure 14a. It can be seen that the Arabian Sea response during July 2003 was characterized by warm anomalies the south of 12°N with a maximum of about 0.4°C in the subsurface at a depth of about 130 m. Anomalous cooling is evident in the top 60 m or so to the south of 8°N in the Arabian Sea. Also seen in Figure 14a is the prominent subsurface cooling, to the north of 14°N in the northern Arabian Sea, which extends well below the mixed layer. On the other hand, the temperature anomalies during July 2002 (Figure 14b) were rather in contrast to those of July 2003. This is evident from the pattern of anomalous subsurface cooling to the south of 12°N and anomalous warming in the northern Arabian Sea (Figure 14b) which is approximately out-of-phase with the pattern of anomalies during July 2003. It may also be noticed that the upper 60–80 m in the southern Arabian Sea was warmer than normal (Figure 14b) in association with the weak monsoonal flow conditions during July 2002. The differences in the temperature anomaly patterns between July 2003 and July 2002 are clearly brought out in Figure 14c. The negative values of the temperature difference in the top 60 m, between the equator and 8°N, are consistent with enhanced surface cooling during 2003 relative to 2002. In the subsurface, the temperature difference pattern shows anomalous warming by as much as 0.5°C, at a depth of about 150 m, which extends between the equator and 12°N. However, the temperature difference to the north of 12°N in the northern Arabian Sea reveals significant cooling which extends vertically through the column. A maximum cooling of about −0.5°C can be seen at a depth of about 80 m around 14°N in Figure 14c. This cooling pattern is suggestive of enhanced upwelling in the northern Arabian Sea during 2003 as compared to 2002. Thus the signatures of the Arabian Sea response associated with the monsoon interannual variability, as seen from the temperature differences between 2002 and 2003, complement the findings based on the analysis of the long-term JEDAC data set which was discussed earlier. In short, the present findings indicate that stronger monsoonal circulations lead to more intense cooling of the mixed layer and warming of the thermocline in the south-central Arabian Sea, accompanied by strong upwelling and enhanced cooling in the northern Arabian Sea. On the other hand, weak monsoonal circulations produce weaker responses of the mixed layer and the thermocline.

5. Discussions and Conclusion

[25] In this paper, we have investigated the role of the southwest monsoon circulation in influencing the interactions between the oceanic mixed layer and the underlying thermocline in the Arabian Sea region. In addition, the study also examines the changes in the upper-ocean response associated with the interannual variability of the southwest monsoon circulation. It is seen from the analysis of ocean temperature data sets that the seasonal surface cooling of the Arabian Sea, during the southwest monsoon months, is accompanied by a distinctive subsurface warming well below the mixed layer with maximum warming at a depth of about 150 m by as much as 1.2°C. A similar feature is observed in the northeast Pacific in association with the strong autumnal forcing [*Large et al.*, 1986]. Analysis of the seasonal cycle of air-sea interactions in the Arabian Sea

region indicates that the strong wind stress forcing and weak vertical density stratification during the southwest monsoon season favor shear instability. Further, it is observed that the Ekman convergence in the central Arabian Sea contributes to downwelling during the southwest monsoon season. In addition, horizontal advective effects in the Arabian Sea are found to be substantial both in the mixed layer and the thermocline in response to the strong monsoonal wind forcing. Offline computations of vertical profiles of heat diffusivity, based on the KPP scheme, clearly show that the vertical diffusion of heat is much stronger and deeper during the southwest monsoon season as compared to other months. Thus the response of the Arabian Sea to the southwest monsoon circulation points to the occurrence of downward transfer of warm waters extending below the mixed layer and provides a plausible mechanism that effectively couples the mixed layer and the thermocline during the summer monsoon season.

[26] Given the seasonal mixed layer cooling and thermocline warming during the southwest monsoon season, we have further examined the changes in the oceanic response due to interannual variations in the monsoonal forcing. Using the long-term ocean temperature data from JEDAC for the period (1955–2001), we have analyzed the interannual variability in the ocean response associated with strong and weak monsoons. On the basis of the present findings, it is explained that the ocean response to strong (weak) monsoonal circulation is characterized by an increase (decrease) in the mixed layer depth in the south-central Arabian Sea. Accordingly, the composite of the ILD (0.8°C) anomalies for strong (weak) monsoon cases show an increase (decrease) in the ILD of about 6–8 m. The corresponding temperature anomalies during strong (weak) monsoons show anomalous cooling (warming) of the mixed layer. On the other hand, the subsurface anomalies for the strong (weak) monsoon composite indicate anomalous warming (cooling) of the thermocline in the south-central Arabian Sea by as much as +0.5°C (−0.5°C). In the northern Arabian Sea, the temperature changes during strong (weak) monsoon years reveal anomalous cooling (warming) due to increased (decreased) upwelling. Furthermore, the ILD anomalies in the northern Arabian Sea, for the strong (weak) monsoon cases, are found to be out-of-phase with those in the south-central Arabian Sea.

[27] We have additionally examined the ocean thermal response associated with the southwest monsoons of 2002 and 2003 using observations from the Argo float network and XBT lines. The in situ observations of subsurface temperatures cover two full summer monsoons seasons of 2002 and 2003, the former being an anomalously weak monsoon and the latter a normal monsoon year. An analysis of subsurface temperature variability during these two years clearly revealed the impact of the monsoon interannual variability on the upper-ocean response. By contrasting the ocean responses associated with monsoons of 2003 and 2002, it is shown that the pattern of mixed layer cooling and thermocline warming was enhanced during 2003 as compared to 2002. While the mixed layer in the south-central Arabian Sea was relatively cooler in 2003 as compared to 2002, the thermocline warming was higher in 2003 by as much as 0.5°C relative to 2002. Owing to enhanced upwelling, the temperature in the northern Arabian Sea was found to be cooler during 2003 relative to 2002. In short, the temperature changes between strong and weak monsoons, as seen from both from JEDAC and Argo data sets, are found to be consistent in manifesting the response of the Arabian Sea to interannual variations in the forcing by the southwest monsoon. While the present study has exclusively focused on the oceanic response to monsoonal forcing, recent studies have raised the possibility of an ocean-atmosphere coupled phenomenon in the tropical Indian Ocean which is analogous to the El Niño–Southern Oscillation in the Pacific Ocean [*Webster et al.*, 1999; *Saji et al.*, 1999]. Further studies will be required to unravel the complex interactions between the coupled instabilities in the Indian Ocean and the monsoon cycle.

[28] **Acknowledgments.** This research work was funded by the Indian Ocean Modeling (INDOMOD) project, Department of Ocean Development (DOD), India. The authors thank the Director, IITM, for providing the infrastructural facilities to carry out this study. We are also thankful to the two anonymous reviewers and the editor for their valuable comments.

References

Bauer, S., G. L. Hitchcock, and D. B. Olson (1991), Influence of monsoonally-forced Ekman dynamics upon surface layer depth and plankton biomass distribution in the Arabian Sea, *Deep Sea Res.*, *38*, 531–553.

Brainerd, K. E., and M. C. Gregg (1995), Surface mixed and mixing layer depths, *Deep Sea Res., Part I*, *9*, 1521–1543.

Conkright, M. E., R. A. Locarnini, H. E. Garcia, T. D. O'Brien, T. P. Boyer, C. Stephens, and J. I. Antonov (2002), World Ocean Atlas 2001: Objective analyses, data statistics, and figures [CD-ROM], report, 17 pp., Natl. Oceanogr. Data Cent., Silver Spring, Md.

Cressman, G. P. (1959), An operational objective analysis system, *Mon. Weather Rev.*, *87*, 367–374.

Derber, J., and A. Rosati (1989), A global oceanic data assimilation system, *J. Phys. Oceanogr.*, *19*, 1333–1347.

Düing, W., and A. Leetmaa (1980), Arabian Sea cooling: A preliminary heat budget, *J. Phys. Oceanogr.*, *10*, 307–312.

Durand, F., S. R. Shetye, J. Vialard, D. Shankar, S. S. C. Shenoi, C. Ethe, and G. Madec (2004), Impact of temperature inversions on SST evolution in the southeastern Arabian Sea during the pre-summer monsoon season, *Geophys. Res. Lett.*, *31*, L01305, doi:10.1029/2003GL018906.

Fischer, A. S., R. A. Weller, D. L. Rudnick, C. C. Eriksen, C. M. Lee, K. H. Brink, C. A. Fox, and R. R. Leben (2002), Mesoscale eddies, coastal upwelling, and the upper-ocean heat budget in the Arabian Sea, *Deep Sea Res., Part II*, *49*, 2231–2264.

Gadgil, S., J. Srinivasan, R. S. Nanjundiah, K. K. Kumar, A. A. Munot, and K. Rupakumar (2002), On forecasting the Indian summer monsoon: The intriguing season of 2002, *Curr. Sci.*, *83*, 394–403.

Joseph, P. V., and P. V. Pillai (1984), Air-sea interaction on a seasonal scale over north Indian Ocean: I. Inter-annual variations of sea surface temperature and Indian summer monsoon rainfall, *Mausam*, *35*(3), 323–330.

Josey, S. A., E. C. Kent, and P. K. Taylor (1999), New insights into the ocean heat budget closure problem from analysis of the SOC air-sea flux climatology, *J. Clim.*, *12*, 2856–2880.

Kalnay, E., et al. (1996), The NCEP/NCAR 40-Year Reanalysis Project, *Bull. Am. Meteorol. Soc.*, *77*, 437–471.

Kara, A. B., P. A. Rochford, and H. E. Hurlburt (2000), An optimal definition for ocean mixed layer depth, *J. Geophys. Res.*, *105*, 16,803–16,822.

Kara, A. B., P. A. Rochford, and H. E. Hurlburt (2003), Mixed layer depth variability over global ocean, *J. Geophys. Res.*, *108*(C3), 3079, doi:10.1029/2000JC000736.

Kara, A. B., H. E. Hurlburt, P. A. Rochford, and J. J. O'Brien (2004), The impact of water turbidity on interannual sea surface temperature simulations in a layered global ocean model, *J. Phys. Oceanogr.*, *34*, 345–359.

Kistler, R., et al. (2001), The NCEP-NCAR 50-Year Reanalysis: Monthly Means CD-ROM and Documentation, *Bull. Am. Meteorol. Soc.*, *82*, 247–268.

Large, W. G., J. C. McWilliams, and P. P. Niiler (1986), Upper ocean thermal response to strong autumnal forcing of the northeast Pacific, *J. Phys. Oceanogr.*, *16*, 1524–1550.

Large, W. G., J. C. McWilliams, and S. C. Doney (1994), Oceanic vertival mixing: A review and a model with a nonlocal boundary layer parameterization, *Rev. Geophys.*, *32*, 363–403.

Large, W. G., G. Danabasoglu, S. C. Doney, and J. C. McWilliams (1997), Sensitivity to surface forcing and boundary layer mixing in a global ocean model: Annual mean climatology, *J. Phys. Oceanogr.*, *27*, 2418–2447.

Lee, C. M., B. H. Jones, K. H. Brink, and A. S. Fischer (2000), The upper-ocean response to monsoonal forcing in the Arabian Sea: Seasonal and spatial variability, *Deep Sea Res., Part II*, *47*, 1177–1226.

Levitus, S., and T. P. Boyer (1994), *World Ocean Atlas 1994*, vol. 4, *Temperature, NOAA Atlas NESDIS 4*, 117 pp., Natl. Oceanic and Atmos. Admin., Silver Spring, Md.

McCreary, J. P., and P. K. Kundu (1989), A numerical investigation of sea surface temperature variability in the Arabian Sea, *J. Geophys. Res.*, *94*, 16,097–16,114.

McCreary, J. P., P. K. Kundu, and R. L. Molinari (1993), A numerical investigation of the dynamics, thermodynamics and mixed layer processes in the Indian Ocean, *Prog. Oceanogr.*, *31*, 181–244.

Meehl, G. A. (1984), A calculation of ocean heat storage and effective ocean surface layer depths for the Northern Hemisphere, *J. Phys. Oceanogr.*, *14*, 1747–1761.

Molinari, R. L., J. Swallow, and J. F. Festa (1986), Evolution of the near-surface thermal structure in the western Indian Ocean during FGGE, 1979, *J. Mar. Res.*, *44*, 739–763.

Murthugudde, R., and A. J. Busalacchi (1999), Interannual variability of the dynamics and thermodynamics of the tropical Indian Ocean, *J. Clim.*, *12*, 2300–2326.

Parthasarathy, B., A. A. Munot, and D. R. Kothawale (1995), All India monthly and seasonal rainfall series: 1871–1994, *Theor. Appl. Climatol.*, *49*, 217–224.

Pegion, P. J., M. A. Bourassa, D. M. Legler, and J. J. O'Brien (2000), Objectively derived daily winds from satellite scatterometer data, *Mon. Weather Rev.*, *128*, 3150–3168.

Prasad, T. G., and M. Ikeda (2001), The wintertime water mass formation in the northern Arabian Sea: A model study, *J. Phys. Oceanogr.*, *32*, 1028–1040.

Rao, R. R. (1987), The observed variability of the cooling and deepening of the mixed layer in the central Arabian Sea during Monsoon-77, *Mausam*, *38*, 43–48.

Rao, R. R., and R. Sivakumar (1999), On the possible mechanisms of the evolution of a mini-warm pool during the pre-summer monsoon season and the onset vortex in the southeastern Arabian Sea, *Q. J. R. Meteorol. Soc.*, *125*, 787–809.

Rao, R. R., and R. Sivakumar (2000), Seasonal variability of near-surface thermal structure and heat budget of the mixed layer of the tropical Indian Ocean from a new global ocean temperature climatology, *J. Geophys. Res.*, *105*, 995–1016.

Rao, R. R., R. L. Molinari, and J. F. Festa (1989), Evolution of the climatological near-surface thermal structure of the tropical Indian Ocean: 1. Description of mean monthly mixed layer depth, and sea surface temperature, surface current and surface meteorological fields, *J. Geophys. Res.*, *94*, 10,801–10,815.

Rochford, P. A., J. C. Kindle, P. C. Gallacher, and R. A. Weller (2000), Sensitivity of Arabian Sea mixed layer to 1994–1995 operational wind products, *J. Geophys. Res.*, *105*, 14,141–14,162.

Rochford, P. A., A. B. Kara, A. J. Wallcraft, and R. A. Arnone (2001), Importance of solar subsurface heating in ocean general circulation models, *J. Geophys. Res.*, *106*, 30,923–30,938.

Roemmich, D., and W. B. Owens (2000), The Argo Project: Global ocean observations for understanding and prediction of climate variability, *Oceanography*, *13*, 45–50.

Saji, N. N., B. N. Goswami, P. N. Vinayachandran, and T. Yamagata (1999), A dipole mode in the tropical Indian Ocean, *Nature*, *401*, 360–363.

Schott, F. (1983), Monsoon response of the Somali Current and associated upwelling, *Prog. Oceanogr.*, *12*, 357–381.

Shenoi, S. S. C., D. Shankar, and S. R. Shetye (2004), Remote forcing annihilates barrier layer in southeastern Arabian Sea, *Geophys. Res. Lett.*, *31*, L05307, doi:10.1029/2003GL019270.

Shetye, S. R. (1986), A model study of the seasonal cycle of the Arabian Sea surface temperature, *J. Mar. Res.*, *44*, 521–542.

Webster, P. J., A. M. Moore, J. P. Loschnigg, and R. R. Leben (1999), Coupled ocean-atmosphere dynamics in the Indian Ocean during 1997–98, *Nature*, *401*, 356–360.

Weller, R. A., M. F. Baumgartner, S. A. Josey, A. S. Fischer, and J. C. Kindle (1998), Atmospheric forcing in the Arabian Sea during 1994–1995: Observations and comparisons with climatology models, *Deep Sea Res., Part I*, *45*, 1961–1999.

Weller, R. A., A. S. Fischer, D. L. Rudnick, C. C. Eriksen, T. D. Dickey, J. Marra, C. Fox, and R. Leben (2002), Moored observations of upper-ocean response to the monsoons in the Arabian Sea during 1994–1995, *Deep Sea Res., Part II*, *49*, 2195–2230.

White, W. B. (1995), Design of a global observing system for gyre-scale upper ocean temperature variability, *Prog. Oceanogr.*, *36*, 169–217.

White, W. B., D. R. Cayan, and J. Lean (1998), Global upper ocean heat storage response to radiative forcing from changing solar irradiance and increasing greenhouse gas/aerosol concentrations, *J. Geophys. Res.*, *103*, 21,355–21,366.

R. Krishnan, Climate and Global Modeling Division, Indian Institute of Tropical Meteorology, Pashan, NCL-Post, Pune, 411008, India. (krish@tropmet.res.in)

K. V. Ramesh, CSIR Centre for Mathematical Modeling and Computer Simulation (C-MMACS), Bangalore-560037, India. (kvram55@yahoo.com)